# Electronic Supplementary Information

# Silver oxide decorated urchin-like microporous organic polymer composites as versatile antibacterial organic coating materials

Yu Zhang*[a,d], Yunxin Tang[b], Qian Liao[b], Yiduo Qian[a], Linglin Zhu[c], Deng-Guang Yu[b], Yixin Xu[a], Xiuhong Lu[a], Il Kim*[e] and Wenliang Song*[b]

[a] School of Pharmacy, Shanghai University of Medicine and Health Sciences, Shanghai 201318, P. R. China

[b] School of Materials and Chemistry, University of Shanghai for Science and Technology, Shanghai 200093, P. R. China.

[c] Department of Oncology, Huadong Hospital Affiliated to Fudan University, No.139 Yan An Xi Road,Shanghai, 200040, PR China.

[d] State Key Laboratory of Molecular Engineering of Polymers, Fudan University, Shanghai 200433, P. R. China

[e] School of Chemical Engineering, Pusan National University, Busan 609-735, Republic of Korea.

*Corresponding author:* Y.Z.: zhangy_21@sumhs.edu.cn *I.K.: ilkim@pusan.ac.kr; W.S.: wenliang@usst.edu.cn*

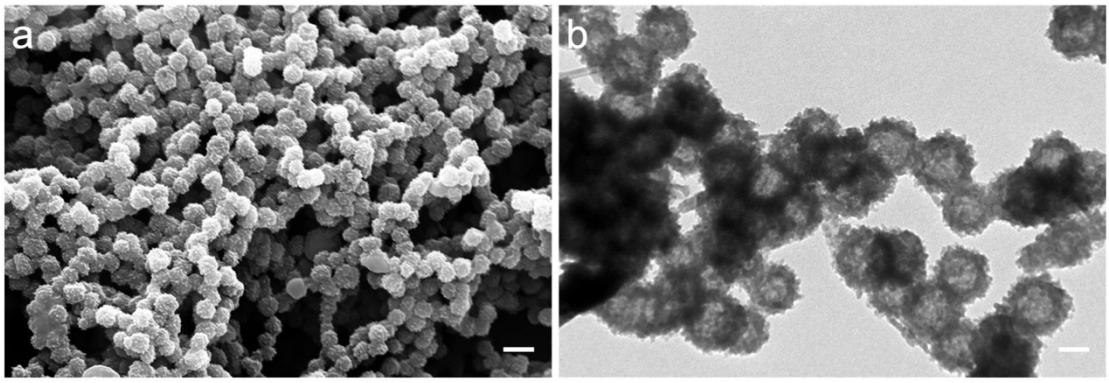

**Figure S1**. (a) Scanning electron microscopy (SEM) and (b) transmission electron microscopy (TEM) images of UMOPs-COOH. Scale bars: 300 nm in a and 100 nm in b. As compared to UMOPs, the sea urchin-like morphology was well-maintained after carboxylation reaction.

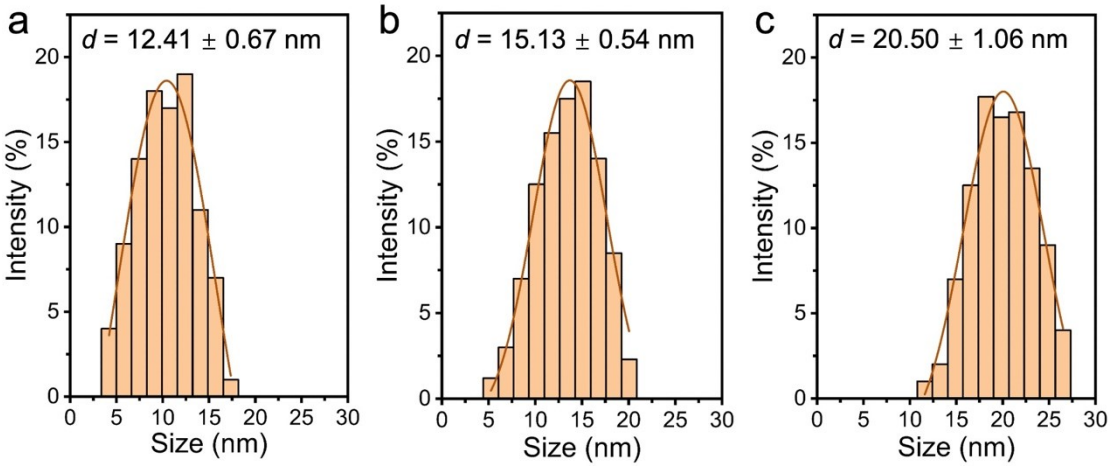


**Figure S2**. Size distribution diagrams of the $Ag_2O$ nanoparticles (NPs) within $Ag_2O$@UMOPs. (a) $Ag_2O$-1@UMOPs, (b) $Ag_2O$-2@UMOPs, and (c) $Ag_2O$-3@UMOPs.

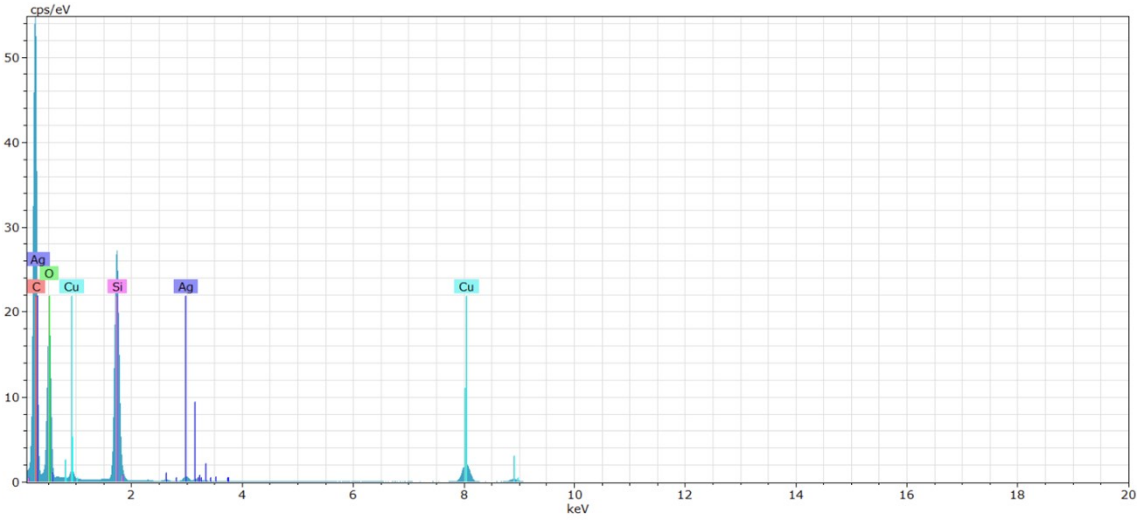


**Figure S3**. Energy-dispersive X-ray spectroscopy (EDX) spectra of $Ag_2O$@UMOPs, the peaks related on the C, O, Ag, Si, Cu, where the Cu peaks are from the mesh of the TEM grids and the Si peak is from the background.

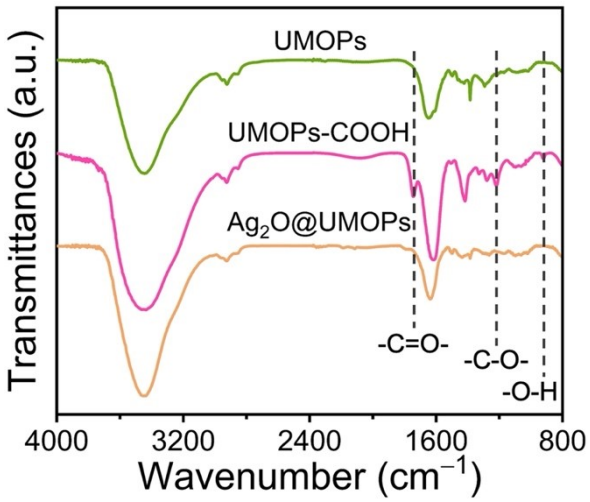


**Figure S4**. FT-IR spectra of UMOPs, UMOPs-COOH, and $Ag_2O$@UMOPs.

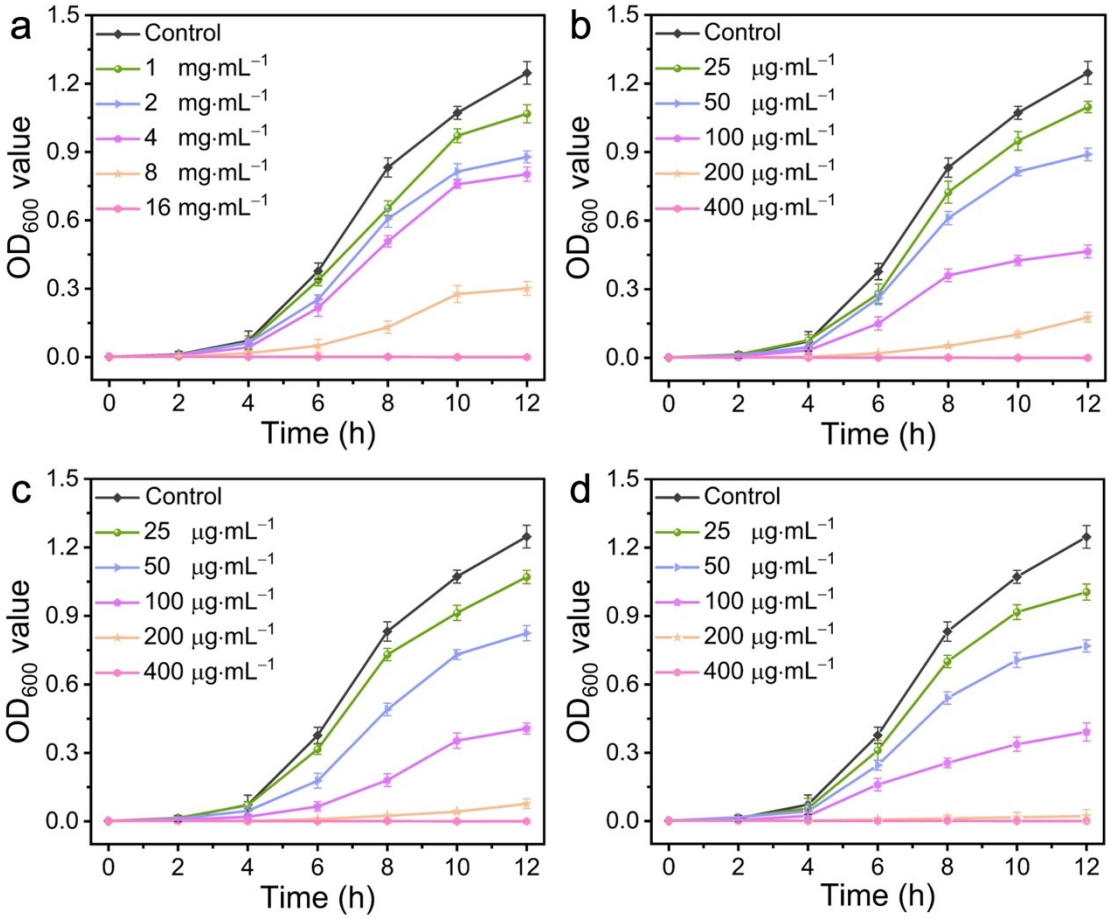


**Figure S5.** Growth curves of *E. coli* treated with different concentrations of (a) UMOPs, (b) $Ag_2O$-1@UMOPs, (c) $Ag_2O$-2@UMOPs, and (d) $Ag_2O$-3@UMOPs.

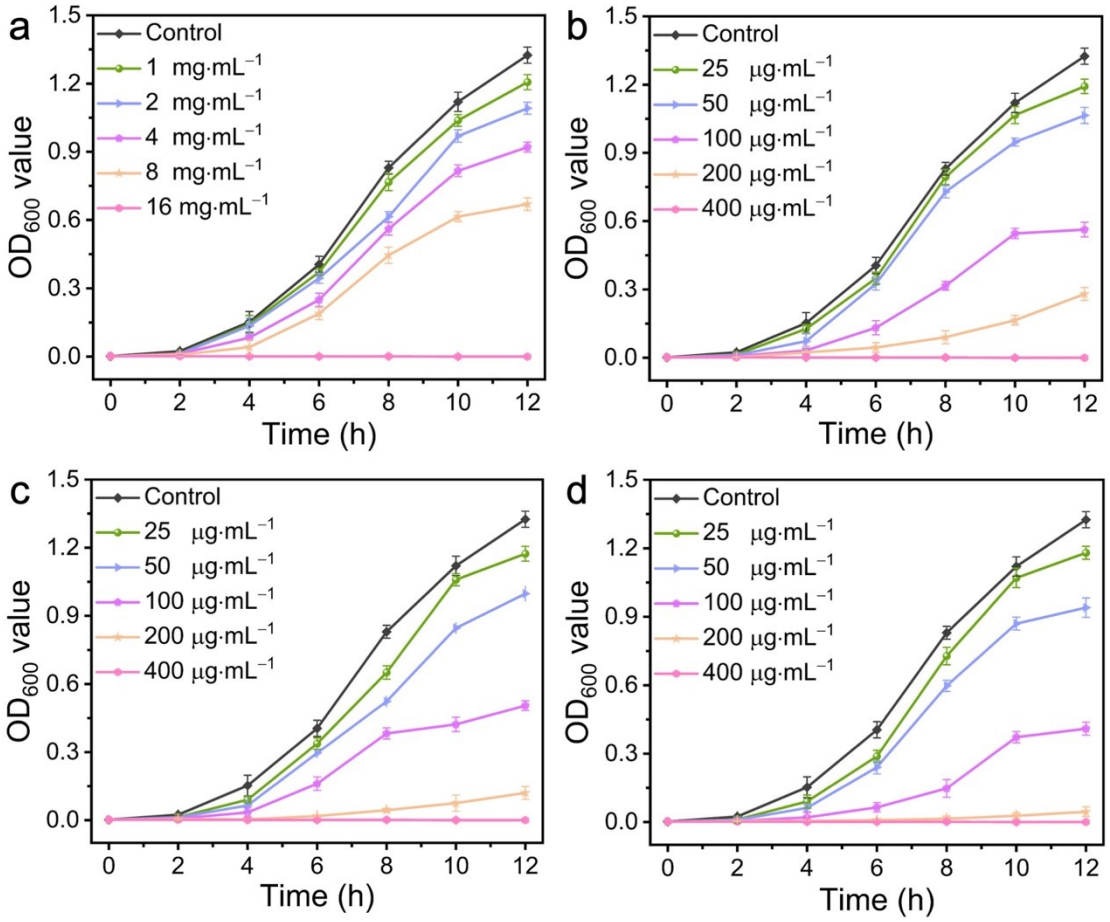


**Figure S6.** Growth curves of *S. aureus* treated with different concentrations of (a) UMOPs, (b) $Ag_2O$-1@UMOPs, (c) $Ag_2O$-2@UMOPs, and (d) $Ag_2O$-3@UMOPs.

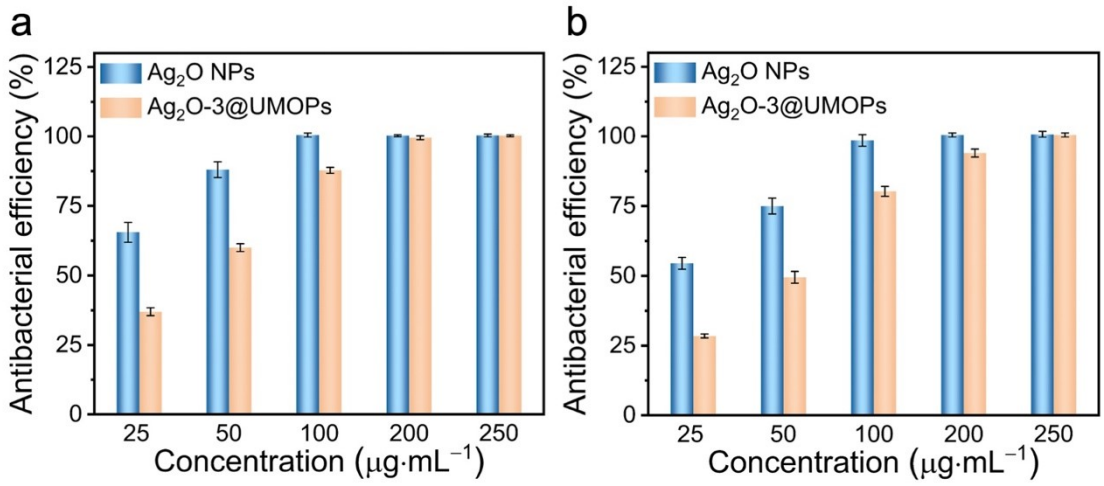


**Figure S7.** Antimicrobial activity of $Ag_2O$ nanoparticles ($Ag_2O$ NPs) and $Ag_2O$-3@UMOPs against (a) *E. coli* and (b) *S. aureus*.

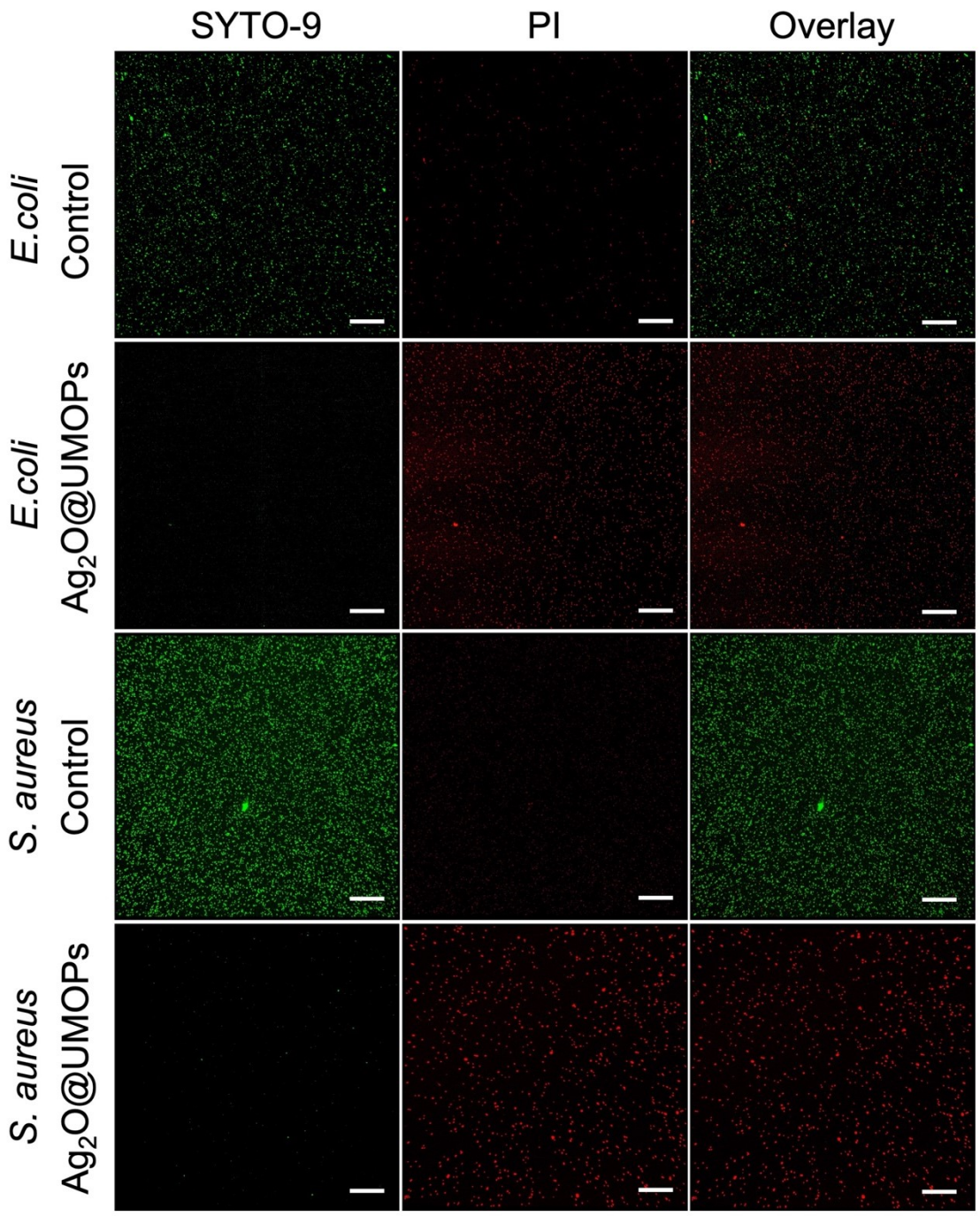


**Figure S8.** Confocal fluorescence microscopic images of control and $Ag_2O$@UMOPs-treated groups of *E. coli* and *S. aureus*. Scale bars: 200 μm.

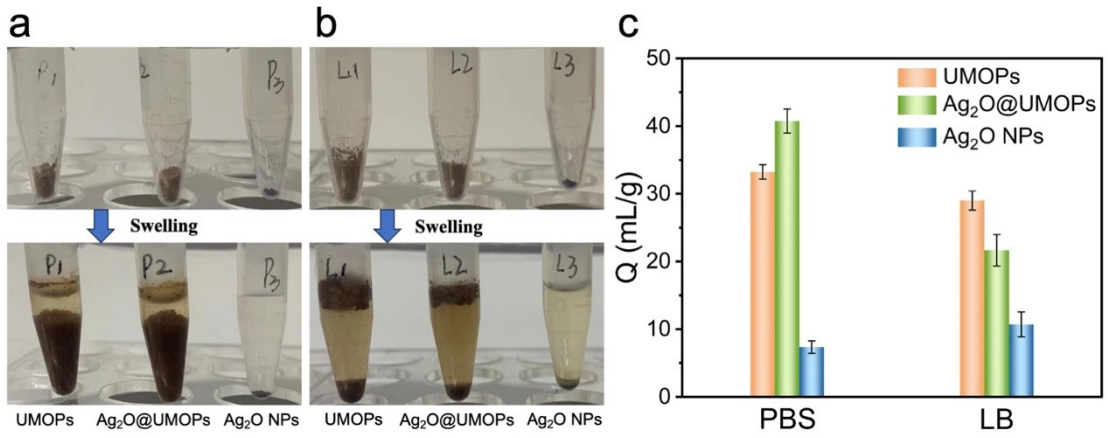


**Figure S9.** Optical photographs showing before and after the swelling of UMOPs, $Ag_2O$@UMOPs and $Ag_2O$ NPs against (a) PBS and (b) LB broth. (c) Swelling ability (Q) of UMOPs, $Ag_2O$@UMOPs and $Ag_2O$ NPs against the specific solvents (The swelling ability was tested by the reported method. The as-prepared UMOPs, $Ag_2O$@UMOPs and $Ag_2O$ NPs (5.0 mg) were placed in an Eppendorf centrifuge tube (1.5 mL), to which was added 0.5 mL of PBS and LB broth. All samples were allowed to stand in the solvents for 24 h, and then the heights of the swollen samples were measured. The heights of the swollen samples were converted to the volume by calculating an empty tube (1.5 mL) with a known volume of water in advance. The swelling ability (Q) of all samples could be determined by the volume of swollen samples (mL) divided by the mass of the samples (0.005 g). The swelling ability experiment on each sample was carried out three times to achieve the average Q values with the error as the standard deviation).

**Table S1.** Comparison of the current study with previously reported data for antibacterial performance

| Materials | Morphology | Size (nm) | Ag content | Thermal stability[b] | Porosity ($m^2/g$)[c] | Antibacterial efficiency Inhibition zone (mm)[d] | Ref. |
|---|---|---|---|---|---|---|---|
| ***$Ag_2O$@UMOPs*** | ***Sea urchin-like morphology*** | ***~200*** | ***3.83 ~ 7.54 wt%*** | **65.03% at 800 ℃** | ***551.26*** | ***S. aureus*: 95.30%**<br>***E.coli*: 99.80%**<br>**200 μg·mL$^{-1}$** | ***This work*** |
| $Ag_2O$@PLLA | Sphere | / | 0.50 wt % | / | / | *S. aureus*: 89.00%<br>*E.coli*: 96.00% | 1 |
| Ag/$Ag_2O$/ZnO@cellulose-chitosan film | / | / | 30.60 ~ 51.30 wt% | 15.57% at 700 ℃ | / | *S. aureus*: 10.00 ~ 19.60<br>*E.coli*: 12.40 ~ 15.00<br>6 mm pieces | 2 |
| $Ag_2O$@LS/CG hydrogel | / | / | 15.00 wt% | 33.00 % at 700 ℃ | / | *S. aureus*: 100.00%<br>*MRSA*: 81.00%<br>1 cm × 1 cm × 0.5 cm | 3 |
| *g*-$C_3N_4$/ZnO-$Ag_2O$ | Irregular layer | / | 3.23 wt% | / | / | *S. aureus*: 10.00 ± 0.50<br>*E.coli*: 7.00 ± 1.00<br>100 μg·mL$^{-1}$ | 4 |
| H-PPAN/rGO-*g*-PAO @$Ag^+$/Ag membrane | Nanofiber | / | / | / | 40.93 | *S. aureus*: 100.00%<br>*E.coli*: 100.00%<br>0.50 g | 5 |

| | | | | | | | |
|---|---|---|---|---|---|---|---|
| AgNPs@P(NIPAM-*co*-MQ) | Sphere | 1 ~ 4 | / | / | / | *S. aureus*: 4.05 μg·mL$^{-1}$<br>*E.coli*: 10.08 μg·mL$^{-1}$<br>MIC[e] | 6 |
| Ag@MSN-QPEI | Sphere | 15 | 3.50 wt % | 29.04% at 790 ℃ | 355.62 | *P.syringae pv. Lachrymans*: 95.19% (40 mg·L$^{-1}$)<br>C.michiganensis subsp. Michiganensis: 95.10 % (50 mg·L$^{-1}$) | 7 |
| IM-POP@Ag | Irregular sphere | / | 26.01 wt% | 66.50% at 800 ℃ | 137.70 | *S. aureus*: 93.66%<br>*E.coli*: 96.56%<br>200 μg·mL$^{-1}$ | 8 |
| rGO-QCP@Ag | Sheet | 3 ~ 4 | 44.07 wt% | 35.05 % at 800 ℃ | / | *S. aureus*: 256 μg·mL$^{-1}$<br>*E.coli*: 16 μg·mL$^{-1}$<br>MIC | 9 |
| polyCu-MOF@AgNPs | Cube | 600 × 100 | 7.24 at%[a] | 27.87% at 700 ℃ | 45.39 | *S. aureus*: 100.00%<br>10 μg·mL$^{-1}$<br>*S. aureus*: 10 μg·mL$^{-1}$<br>MIC | 10 |

[a] Atomic ratio; [b] Weight residue after thermal degradation; [c] The highest BET surface areas reported in the article; [d] The highest antibacterial efficiency or the largest inhibition zone reported in the article; [e] Minimal inhibition concentrations.

**Table S2**. Summary of the elemental content for UMOPs and $Ag_2O$@UMOPs

| Element (at%) | C | O | Ag |
|---|---|---|---|
| UMOPs | 91.87 | 8.13 | 0.00 |
| $Ag_2O$-1@UMOPs | 88.41 | 11.02 | 0.57 |
| $Ag_2O$-2@UMOPs | 87.84 | 11.21 | 0.95 |
| $Ag_2O$-3@UMOPs | 87.15 | 11.73 | 1.12 |

The data is from the XPS analysis.

**Reference**

[1] E. Lizundia, I. Armentano, F. Luzi, F. Bertoglio, E. Restivo, L. Visai, L. Torre, D. Puglia, Synergic effect of nanolignin and metal oxide nanoparticles into poly (L-lactide) bionanocomposites: material properties, antioxidant activity, and antibacterial performance, *ACS Appl. Bio Mater.*, 2020, **3**, 5263-5274.

[2] Y. Peng, H. Zhou, Y. Wu, Z. Ma, R. Zhang, H. Tu, L. Jiang, A new strategy to construct cellulose-chitosan films supporting Ag/$Ag_2O$/ZnO heterostructures for high photocatalytic and antibacterial performance, *J. Colloid Interface Sci.*, 2022, **609**, 188-199.

[3] X. Xie, M. Zhang, Y. Li, Y. Lei, J. Sun, N. Sattorov, K. B. Makhmudov, J. Wang, NIR as a "trigger switch" for situ distinguish superbacteria and photothermal synergistic antibacterial treatment with $Ag_2O$ particles/lignosulfonate/cationic guar gum hybrid hydrogel, *Int. J. Biol. Macromol.*, 2023, **232**, 123340.

[4] S. Vignesh, P. Eniya, M. Srinivasan, J. K. Sundar, H. Li, S. Jayavel, M. Pandiaraman, M. A. Manthrammel, M. Shkir, B. Palanivel, Fabrication of Ag/$Ag_2O$

incorporated graphitic carbon nitride based ZnO nanocomposite for enhanced Z-scheme photocatalytic performance of various organic pollutants and bacterial disinfection, *J. Environ. Chem. Eng.*, 2021, **9**, 105996.

[5] N. Han, W. Wang, X. Lv, W. Zhang, C. Yang, M. Wang, X. Kou, L. Wei, Y. Dai, X. Zhang, Highly efficient purification of multicomponent wastewater by electrospinning kidney-bean-skin-like porous H-PPAN/rGO-*g*-PAO@ $Ag^{+}$/Ag composite nanofibrous membranes, *ACS Appl. Mater. Interfaces*, 2019, **11**, 46920-46929.

[6] H. Ji, S. Zhou, Y. Fu, Y. Wang, J. Mi, T. Lu, X. Wang, C. Lü, Size-controllable preparation and antibacterial mechanism of thermo-responsive copolymer-stabilized silver nanoparticles with high antimicrobial activity, *Mater. Sci. Eng. C*, 2020, **110**, 110735.

[7] J. Niu, G. Tang, J. Tang, J. Yang, Z. Zhou, Y. Gao, X. Chen, Y. Tian, Y. Li, J. Li, Y. Cao, Functionalized silver nanocapsules with improved antibacterial activity using silica shells modified with quaternary ammonium polyethyleneimine as a bacterial cell-targeting agent, *J. Agric. Food Chem.*, 2021, **69**, 6485-6494.

[8] H. Luo, T. Huang, X. Li, J. Wang, T. Lv, W. Tan, F. Gao, J. Zhang, B. Zhou, Synergistic antibacterial and wound-healing applications of an imidazole-based porous organic polymer encapsulated silver nanoparticles composite, *Microporous Mesoporous Mater.*, 2022, **337**, 111925.

[9] S. Zhou, H. Ji, Y. Fu, Y. Yang, C. Lü, Mussel-inspired fabrication of cationic polymer modified rGO supported silver nanoparticles hybrid with robust antibacterial

and catalytic reduction performance, *Appl. Surf. Sci.*, 2020, **506**, 144655.

[10] C. Guo, F. Cheng, G. Liang, S. Zhang, Q. Jia, L. He, S. Duan, Y. Fu, Z. Zhang, M. Du, Copper-based polymer-metal–organic framework embedded with Ag nanoparticles: Long-acting and intelligent antibacterial activity and accelerated wound healing, *Chem. Eng. J.*, 2022, **435**, 134915.